



Multi Metal Ion Recognizing Unsymmetrical tetra dentate Schiff bases Associated with Antifungal activity

SELVARAJ SHUNMUGAPERUMAL¹, SARANYA DHASARATHAN¹,
KAMATCHI SELVARAJ. P^{1*} and ILANGO KALIAPPAN²

¹Department of Chemistry, Government Arts College for Men (Autonomous), Nandanam, Chennai-600 035, Tamil Nadu, India.

²Department of Pharmaceutical Chemistry, SRM College of Pharmacy, SRM Institute of Science and Technology, Kattankulathur-603 203, Chengalpattu District, Tamil Nadu, India.

*Corresponding author E-mail: porbal96@gmail.com

<http://dx.doi.org/10.13005/ojc/370410>

(Received: July 07, 2021; Accepted: August 08, 2021)

ABSTRACT

New unsymmetrical Schiff bases containing azomethine moiety with simple aromatic section in one side and ferrocene fragment attached imine on the other side have been synthesized. Advent of metal-to-ligand charge transfer band for the coordination of Cu²⁺ ions with receptors and appropriate changes in UV-Visible spectra for other metal ion combination with the sensor is reported. Observed extravagant ΔE_p values suggest quasi-reversible process. The ΔI_{pa} amount calculated from the anodic current I_{pa} value noticed for receptor solution and different metal ion added sensor solution discloses the concentration of metal ions required for effective sensing. The synthesized ligands were subjected to antimicrobial activity against four bacterial and two fungal stains and the zone of inhibition (in mm) was calculated. Further molecular docking study was carried out and the binding energy (Kcal.mol⁻¹) for the synthesized ligand (R₁ and R₂) with the selected protein was intended.

Keywords: Azomethine, Cation sensors, Binding attitude, Molecular docking, MLCT Band, Unsymmetrical Schiff base.

INTRODUCTION

Researchers are interested to develop selective chemosensors to identify the trace amount of transition metal ions involved in many biological processes. Not only have that, the influence of metal ions having redox behavior in the environment also captivated the attraction of scientist to synthesize sensor compounds capable of identifying different metal ions¹. Qualities like non-destructive nature,

easiness in synthesis, selectiveness towards target entities, quick retention time and capability to diagnose biological samples² project chemosensors to unique place rather than the other instrumental method of analysis³.

Preparation of sensors proficient in identifying cations in solution and converting the action of recognition in to documentable signal are of flourishing field with enormous amount of published



works⁴. Interlocking ability of the synthesized compounds with hazardous heavy metal cations and anions hinge on the π electrons cloud available on C=N group which in turn is influenced by heterocyclic aromatic part with nitrogen and inductive effect of substituent groups⁵. Metal-to-Ligand charge-transfer and intramolecular charge transfer may emerge for the union of sensor and targeted ions⁶.

Copper ions control the biological activity of cytochrome c oxidase, superoxide dismutase and tyrosinase enzymes. Despite, higher insertion modify the functions of enzymes and lead to antagonistic actions like, lethargy, hike in blood pressure, nausea and Alzheimer's diseases⁷. Solubility of Hg^{2+} in water makes it to penetrate through membrane of the cell leading to malfunction of brain, letdown of kidney functions, infirmity of neuro system and Minamata disease⁸. Consumption of chocolate, milk and cookies made of milk, canned food and hydrogenated oils induces Ni^{2+} ion in biological systems. Development of cancer in respiratory organs, pneumonia, asthma and malfunctioning of nervous system has been reported⁹ for the excess intake of Ni^{2+} ions.

Consumption of Cd^{2+} ions toxicity prompts productivity, hepatic and cardiovascular dysfunctions¹⁰. Harmfulness of Pb^{2+} ion exposure include procreative malady in human, neurological dysfunctions and loss of strength at bone joints¹¹. Health hazards persuaded by manganese toxicity include damage to immune system, central nervous system, kidney function and exocrine & endocrine function of pancreas¹².

Here in we report the synthesis of new unsymmetrical Schiff bases N' -((E)-2-nitrobenzylidene)-2-((E)-2-(ferrocenylidene)hydrazine-1-carbothiohydrazide and N' -((E)-2-hydroxy-5-nitrobenzylidene)-2-((E)-2-(ferrocenylidene)hydrazine-1-carbothiohydrazide containing aromatic part at one end and ferrocene compound at the other end of the main frame structure. Spectroscopic and redox studies exposes that synthesized receptor possess sensing aptitude towards metal ions like, Hg^{2+} , Mn^{2+} , Pb^{2+} , Cd^{2+} , Ni^{2+} and Cu^{2+} .

Reported literature¹³ discloses that the biological and chemical activities of Schiff bases depend upon the sp^2 hybridized nitrogen donor atom of the azomethine group. The proteins present in microorganisms find suitability to form hydrogen bond with the active site of azomethine group containing high electro negative nitrogen atom, which in turn is responsible for the anticancer, antibacterial and antifungal activities¹⁴. Prokaryotic nature of bacteria (unicellular organism without nucleus, cell wall & organelles and survives on the host entities) helps to develop enormous amount of antibacterial commixture whereas eukaryotic nature of fungi (multicellular organism with nucleus, cell wall & organelles and endures independently) prevent the formulation of antifungal agents¹⁵. The newly synthesized sensor by us exhibit better antifungal activity rather than antibacterial activities.

EXPERIMENTAL

Materials

Chemicals [AR grade] such as carbon disulfide, 2-hydroxy-5-nitrobenzaldehyde, ferrocene carboxaldehyde, hydrazinehydrate, 2-nitrobenzaldehyde and silica gel were purchased from E.Merck industry. They were used without further purification. Analytical grade NiCl_2 , MnCl_2 , CuCl_2 , HgCl_2 , $\text{Pb}(\text{OAc})_2$ and $\text{Cd}(\text{OAc})_2$ used in the electronic spectral and CV studies were procured from Sigma-Aldrich. Acetonitrile [HPLC grade] obtained from E-Merck and absolute ethanol [spectral grade] acquired from Commercial Alcohols, Canada was used for spectral studies. Tetrabutylammoniumperchlorate [99+%] secured from Chemical Center, Mumbai was used as such without purification.

Instruments

Bruker Daltonics esquire 3000 spectrometer was used to record mass spectra. BRUKER AVANCE spectrometer [500 MHz] engaging $\text{C}_2\text{D}_5\text{OD}$ solvent was adopted to document proton NMR spectra. Perkin-Elmer 337 spectrometer was engaged to register FTIR spectra in the range of $400\text{-}4000\text{ cm}^{-1}$ using KBr pellets. SHIMADZU MODEL UV-1800 240V spectrophotometer was affianced to observe UV-Visible spectral studies between 200 and 800 nm. CHI electrochemical

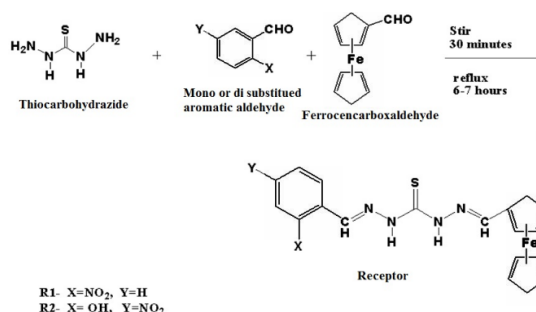
analyzer 1200B model was employed to draw cyclic voltammograms using platinum as counter electrode, Ag/AgCl as reference electrode and glassy carbon as working electrode. The C, H and N contents were analyzed with Herarus C-H-N rapid analyzer.

Synthesis of *N'*-((*E*)-2-Nitrobenzylidene)-2-((*E*)-2-(ferrocenylidene)hydrazine-1-carbothiohydrazide [R1]

Hydrazinehydrate and carbon disulphide in 3:1 molar ratio was refluxed for ten hours at 80°C along with 0.15 mole of 2-chloroethanol as catalyst to prepare the precursor compound thiocarbonylhydrazide¹⁶. To a clear solution [0.01 mole/25 mL] of purified thiocarbonylhydrazide in ethanol, a mixture of 2-nitrobenzaldehyde (0.01mol) and ferrocene carboxaldehyde (0.01 mol) in 180 mL ethanol was added. After half an hour stirring, the reaction mixture was refluxed for 6-7 hours. Thin layer chromatographic technique was used to check the progress of the reaction at various time intervals. Filtration was carried out after cooling and the filtrate was concentrated to get reddish yellow colored *N'*-((*E*)-2-Nitrobenzylidene)-2-((*E*)-2-(ferrocenylidene)hydrazine-1-carbothiohydrazide. Column having silica gel as stationary phase was used for the purification of crude sample. Ethanol was used as eluent. Color: Dark reddish orange. Yield: 0.538 g (91%), m.p. 69°C.

Synthesis of *N'*-((*E*)-2-hydroxy-5-nitrobenzylidene)-2-((*E*)-2-(ferrocenylidene)hydrazine-1-carbothiohydrazide [R2]

Solution containing 0.01 mole of thiocarbonylhydrazide in 25 mL of ethanol was added with stirring to another solution having 0.01 mole of 2-hydroxy-5-nitrobenzaldehyde and 0.01 mole of ferrocene carboxaldehyde in 180 mL ethanol. The reaction mixture was stirred for another half an hour and then refluxed for 6-7 hours. The progress of the reaction at various time intervals was checked using thin layer chromatographic technique. The reaction mixture was filtered after cooling. Greenish yellow color solid was obtained after concentrating the filtrate. The product was further purified by column chromatography using silica gel as stationary phase and ethanol as eluent. Yield: 0.5442 g, (91%), Color: reddish yellow, m.p. 70°C.



Scheme of Synthesis

- R1-*N'*-((*E*)-2-Nitrobenzylidene)-2-((*E*)-2-(ferrocenylidene)hydrazine-1-carbothiohydrazide
R2-*N'*-((*E*)-2-hydroxy-5-nitrobenzylidene)-2-((*E*)-2-(ferrocenylidene)hydrazine-1-carbothiohydrazide

In-vitro activities for microorganisms

Antimicrobial studies were carried out in triplicate (*in-vitro*) for the synthesized ligands by standard method¹⁷ against four bacteria at 37°C and two fungi at room temperature.

Molecular docking studies

The molecular docking study was carried out using Auto dock version 4.2.6¹⁸ to investigate the binding mode of the synthesized compounds R1 and R2 with the target protein. The 3D crystal structure with Protein Data Bank PDB code 1PTF (*Streptococcus faecalis*), 6KVQ (*Staphylococcus aureus*), 7BU2 (*Escherichia coli*), 4YXB (*Salmonella typhimurium*) 3K4Q (*Aspergillus niger*), 6TZ6 *Candida albicans*) was used as target protein and it was extracted from Research Collaboratory for Structural Bioinformatics (www.RCSB.org). Molecular Graphics Laboratory (MGL) tools of Auto dock were employed to get the docking score. Engaging 3D optimization tool, the structures of the compounds R1 and R2 were drawn using ChemSketch and converted to 3D structure. Geometrical optimization of ligands using ligand module was implemented using Molecular Mechanics Force Field 94 (MMFF94) as implemented in the software. The analysis was done by docking the prepared ligand with the selected protein for its affinity towards the particular amino acid residue present and calculated the H-bond interaction and binding energy (K Cal/mole).

Elemental and Mass Spectral analysis

The data obtained on elemental analysis of the synthesized compounds matches very well with

the theoretical values. R1 (Found: C, 50.61; H, 3.73; N, 15.51; Fe, 12.18; Calc. for $C_{19}H_{17}N_5O_2SFe$: C, 50.66; H, 3.77; N, 15.55; Fe, 12.20 %). R2 (Found: C, 50.59; H, 3.70; N, 15.47; Fe, 12.16; Calc. for $C_{19}H_{17}N_5O_3SFe$: C, 50.66; H, 3.77; N, 15.55; Fe, 12.20 %).

On mass spectral analysis, the advent of molecular peak (ESI) m/z at 434 and 450 respectively for the compounds $N'((E)-2\text{-Nitrobenzylidene})-2-((E)-2\text{-ferrocenylidene})\text{hydrazine-1-carbothiohydrazide}$ & $N'((E)-2\text{-hydroxy-5-nitrobenzylidene})-2-((E)-2\text{-ferrocenylidene})\text{hydrazine-1-carbothiohydrazide}$ confirm the formation of expected receptors.

FTIR Spectral analysis

In the FTIR spectrum of compound R1 (Fig. 1), the peak observed around 500 cm^{-1} and 830 cm^{-1} are assigned to ferrocene cyclopentadienyl ring tilt stretching vibration and C-H out of plane bend vibrations respectively¹⁹. The peak positioned between 900 cm^{-1} to 1080 cm^{-1} are allocated to the $\delta\text{-C-C-H}$ bending vibration in the penta cyclic ring. The peak at 1104 cm^{-1} is allotted for breathing ring deformation²⁰ vibration. The peaks appeared at 1340 cm^{-1} , 1519 cm^{-1} and 1567 cm^{-1} are assigned for C=S group stretching vibration, C-C stretching vibration of pentacyclic ring and NO_2 group vibration respectively. The appearance of -C=N stretching vibration peak at 1650 cm^{-1} confirms the formation of Schiff base and is lower than the vibration frequency of -C=O group of the -CHO group present in ferrocene (1678 cm^{-1})¹⁹. The absorption peak emerged at 2059 cm^{-1} has been earmarked for aromatic stretching vibration. The peaks observed between $3200 - 3400\text{ cm}^{-1}$ is attributed to stretching vibration of secondary amine and water of hydration. Compound R2 also give the above mentioned peaks and the stretching vibrational modes of phenolic -OH appears along with secondary amine and water of hydration peaks in $3200 - 3400\text{ cm}^{-1}$ region itself²¹.

NMR Spectral analysis

The proton NMR spectrum of R1 in $\text{C}_2\text{D}_5\text{OD}$ solvent (Fig. 2) contains relevant peaks and are assigned accordingly δ ,(ppm) 8.4(s, 2H, NCH), 7.8 (m, 4H aromatic), 4.8(m, 2H, (cp(subst.)), 4.4(m, 2H, (cp(subst.)), 4.2(s, 5H, (cp(unsubst.)), 1.19 (s, 2H, 2NH). For compound R2 alike spectral peaks

8.4(m, 2H, NCH), 8.3 (s, 1H, aromatic), 8.1(s, 1H, aromatic), 7.0 (s, 1H,Ar), 4.4(m, 4H, (cp(subst.)), 4.2 (m, 2H, (cp(unsubst.)), 3.9(s, 5H, cp unsubst), 1.14(s,2H, NH), along with a prominent singlet at δ 5.0(s, phenolic-OH) appear in the spectrum.

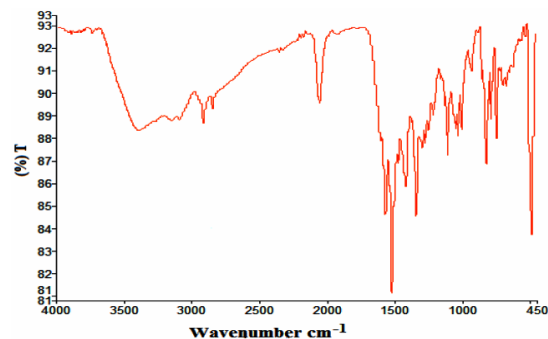


Fig. 1. FTIR spectrum of R1

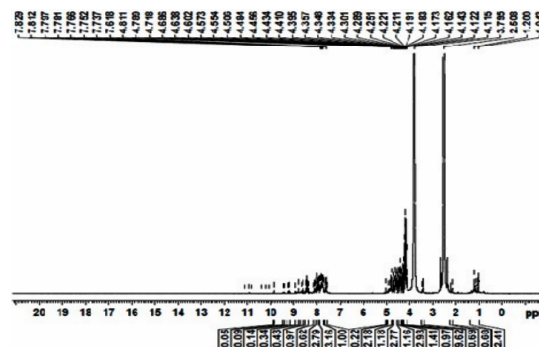


Fig. 2. Proton NMR spectrum of R1

RESULTS AND DISCUSSION

Investigation of sensing nature of receptors

Exploration of the ability of receptors to imprisonment with the various metal ions was carried out by titration method while recording the UV-Visible spectra. Twenty μL aliquots of metal solutions (10^{-2} M) were added to 2.5 mL of receptor solution (10^{-5} M) taken in the quartz cell. Since, chloride salts of copper, mercury and nickel are soluble in acetonitrile, solution of the receptor in acetonitrile was used for the above three metal salt solutions. Alcoholic solution of receptors was used for the chloride salts of manganese and acetate salts of lead & cadmium as these salts are soluble in ethanol. In acetonitrile R1 shows two shoulders around 259 nm and 313 nm (Fig. 3a). Alcoholic solution of R1 displays three peaks near 205 nm, 243 nm and 313 nm (Fig. 3b). Aromatic ring $\pi\text{-}\pi^*$ transitions are assigned for above observation²².

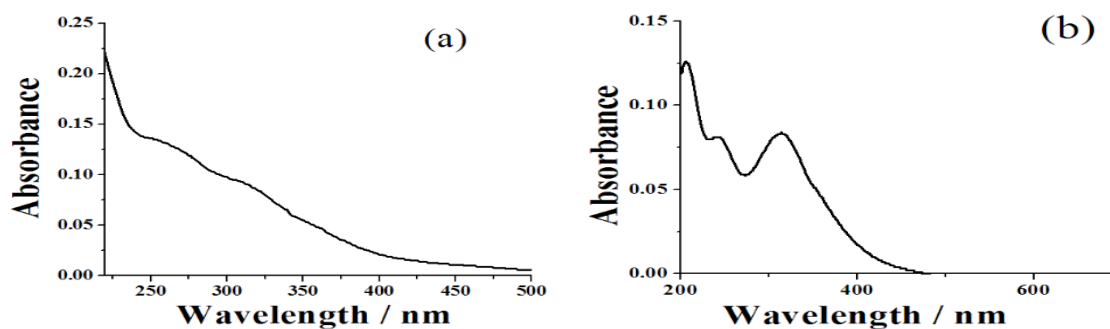


Fig. 3. Electronic spectra of R1 in a) acetonitrile b) ethanol

Effective coordination of Cu^{2+} ions with receptor is exposed by the development of new prominent peaks around 305 nm, 350 nm and 460 nm (Fig. 4a). The 460 nm peak (Fig. 4b) has been assigned²³ for MLCT band which has

developed after the coordination of Cu^{2+} ions with receptor. Development of additional peaks near 305 nm and 350 nm (Fig. 4c) at the expenses of the shoulder peaks of receptor also ascertain the sensing capacity of R1.

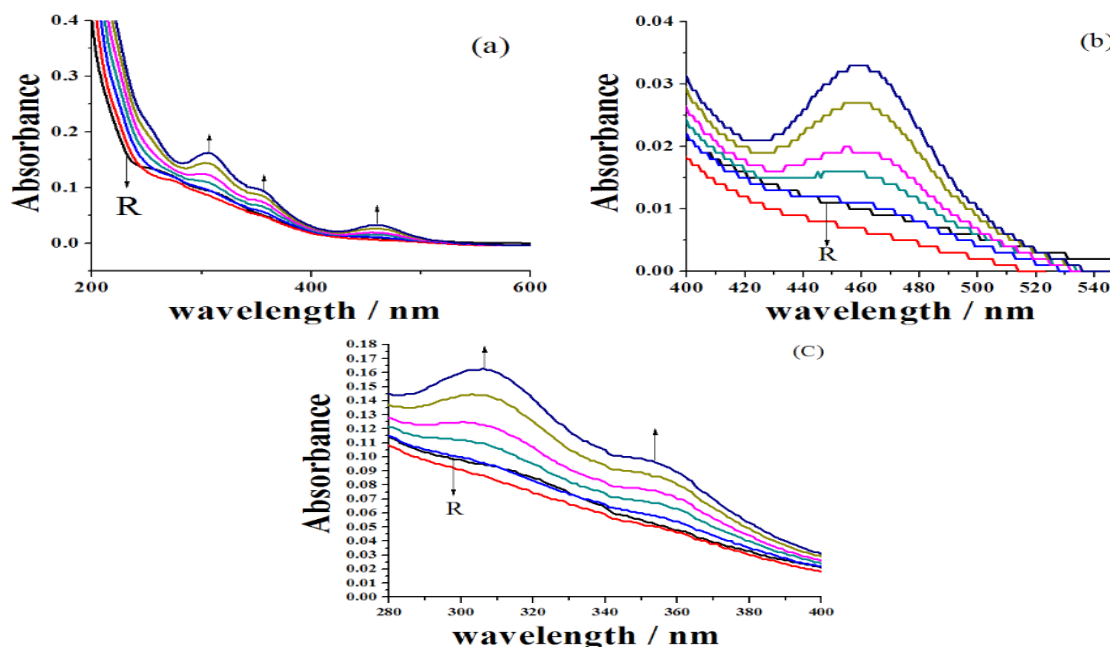


Fig. 4. Spectral changes noticed for the addition of Cu^{2+} ion to R1 a) Overall changes b) Formation of MLCT band c) Development additional peaks near 305 nm and 350 nm

Successive addition of Hg^{2+} ions generate new peak around 237 nm (Fig. 5a) and Pb^{2+} ions cause overall blue shift for all the base peaks (Fig. 5b) of the receptor R1. Similarly consecutive addition of Ni^{2+} ions gives a shoulder around 269 nm (Fig. 5c). Increase in absorbance value is noticed in the overall wavelength region for cumulative addition of Mn^{2+} and for Cd^{2+} ions along with the disappearance of shoulder at 243 nm²².

Aromatic ring π - π^* transition of R2 appear as a shoulder around 298 nm in acetonitrile and as

a prominent peak at 313 nm in ethanol (Figure. 6).

Spectral changes observed for the addition of Cu^{2+} ions to R2 also generate peaks near 303 nm, 354 nm and 460 nm (Fig. 7a,b,c), which confirms that R2 is efficiently sensing the Cu^{2+} ions.

Discerning ability of R2 towards Hg^{2+} , Ni^{2+} and Pb^{2+} ions is exposed by the formation of new peak at 230 nm for Hg^{2+} (Fig. 8a), blue shift of 298 nm shoulder to 278 nm for Ni^{2+} (Fig. 8b) and conversion of 313 nm peak to a broad shoulder at the same wavelength (Figure 8c).

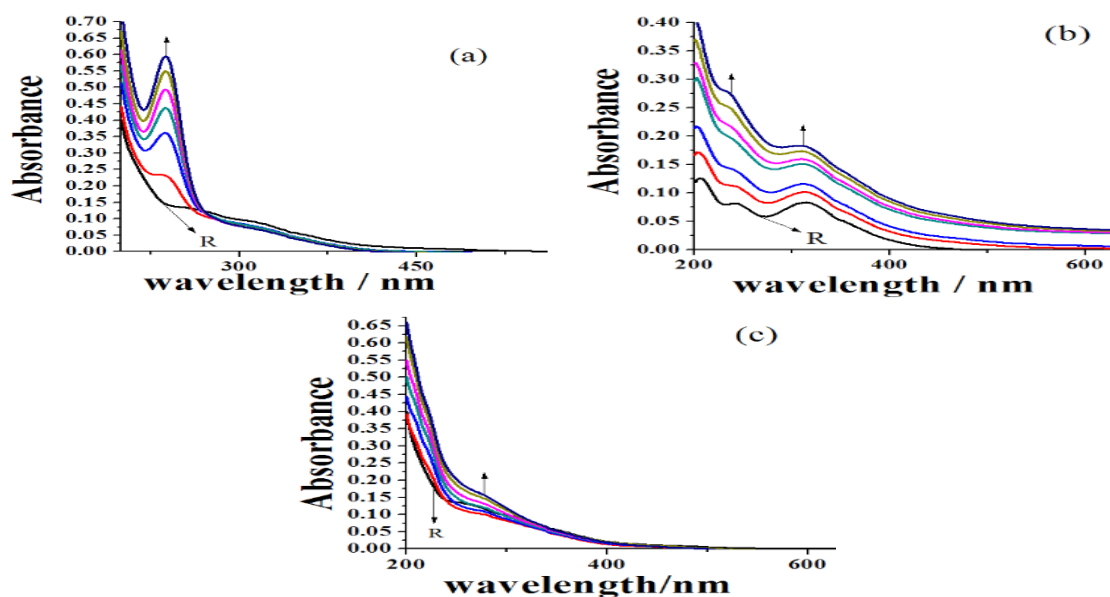


Fig. 5. Spectral changes noticed for R1 with the addition of a) Hg^{2+} ions b) Pb^{2+} ions c) Ni^{2+} ions

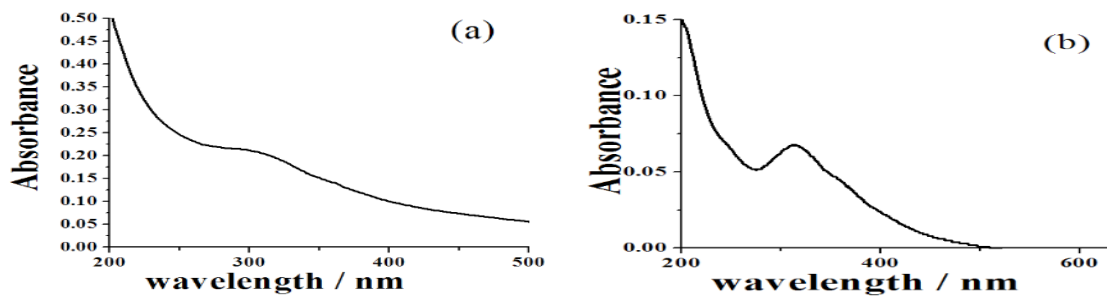


Fig. 6. UV-Visible spectrum of R2 in a) acetonitrile b) ethanol

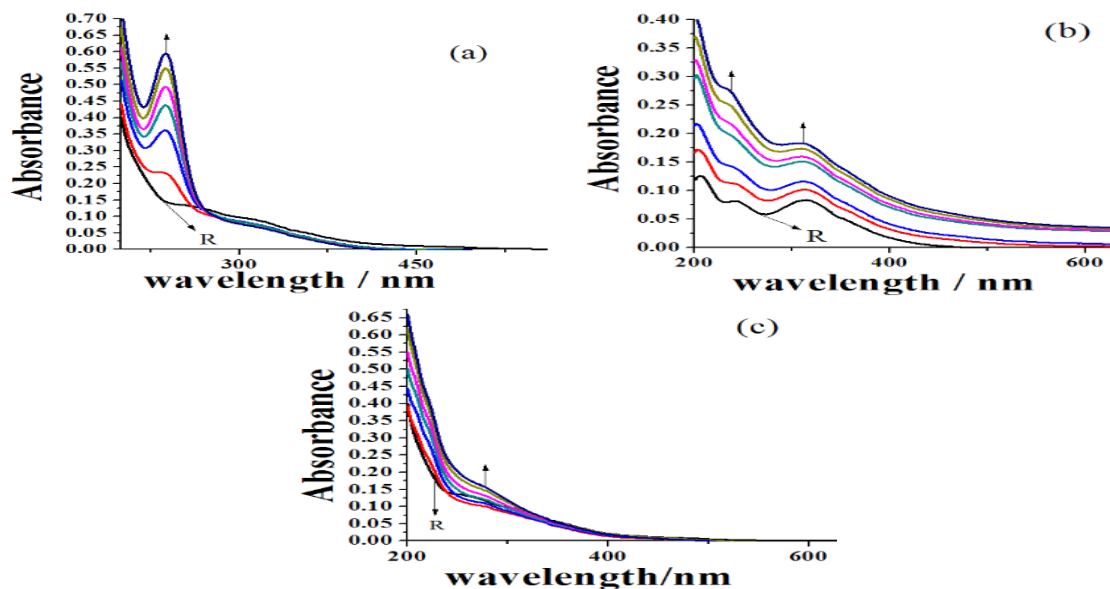


Fig. 7. Change in the absorbance spectrum of R2 with Cu^{2+} ions a) overall changes b) formation of MLCT band c) generation of new peaks at 303 nm and 354 nm

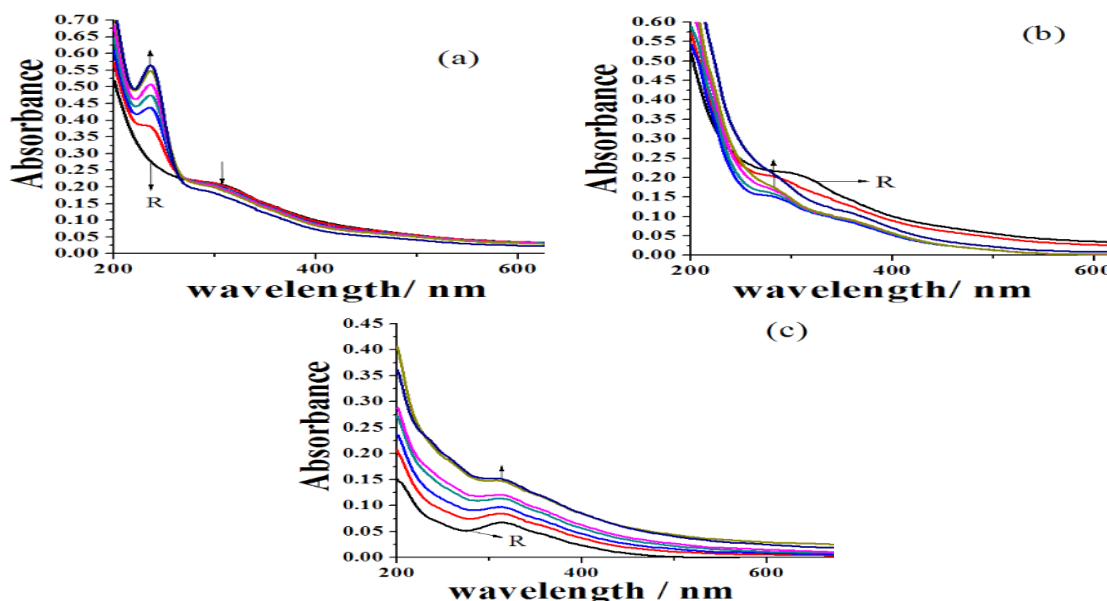


Fig. 8. Discerning ability of R2 towards a) Hg^{2+} ions, b) Ni^{2+} ions, c) Pb^{2+} ions

Interaction studies with cyclic voltammetry

Responses to the applied potential were documented in cyclic voltammetry to establish the sensing priority order. Increasing ΔE_p , I_{pa} & I_{pc} values (Table 1) noticed in the voltammograms

recorded with different scan rate (20, 50 & 100 mV/sec) for metal free R1 (Fig. 9) and overblowed ΔE_p values (99-140 mV other than the expected 59 mV) emphasized the quasi-reversible one-electron redox process²⁴.

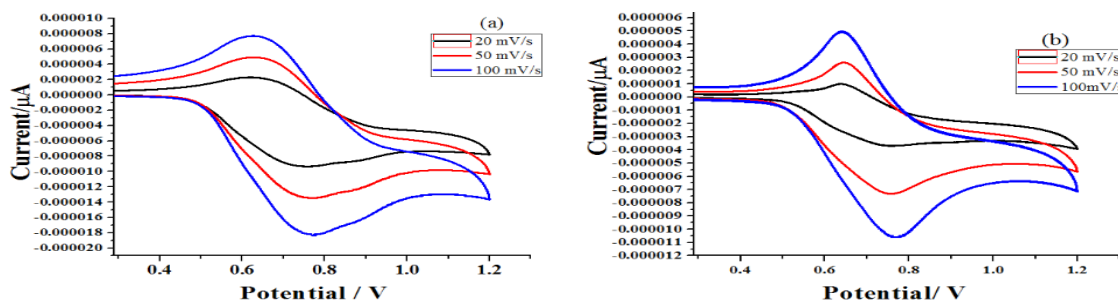


Fig. 9. Cyclic voltammograms of R1 (1×10^{-3} M) with different scan rate in a) acetonitrile b) ethanol

Table 1: Electrochemical parameters for R1

Scan Rate-mV/ sec	E_{pa} (V)	E_{pc} (V)	ΔE_p (V)	$E_{1/2}$ (V)	$I_{pa} \times 10^{-5}$ (μA)	$I_{pc} \times 10^{-5}$ (μA)
Solvent -Acetonitrile						
20	0.749	0.634	0.115	0.692	-0.928	0.224
50	0.76	0.632	0.128	0.696	-1.346	0.495
100	0.764	0.623	0.14	0.694	-1.818	0.774
Solvent - Ethanol						
20	0.743	0.636	0.107	0.689	-0.371	0.09
50	0.75	0.651	0.099	0.7	-0.627	0.259
100	0.768	0.638	0.13	0.703	-1.059	0.487

The detected positive potential shift for oxidation peak and negative potential shift for reduction peak²⁵⁻²⁶ in the voltammograms logged in the CV titration (to 10 mL of 10^{-3} molar R1 solution 20 μL of 10^{-3} molar metal solution were added up to 7eq)

under equimolar (10^{-3} R1/ 10^{-3} M^{2+}) and multimolar (10^{-3} R1/ 10^{-1} M^{2+}) concentration reveals that the synthesized receptors is capable of sensing deferent metal ions. Fig. 10 chronicled for the addition of Cd^{2+} ions is presented here as a reference.

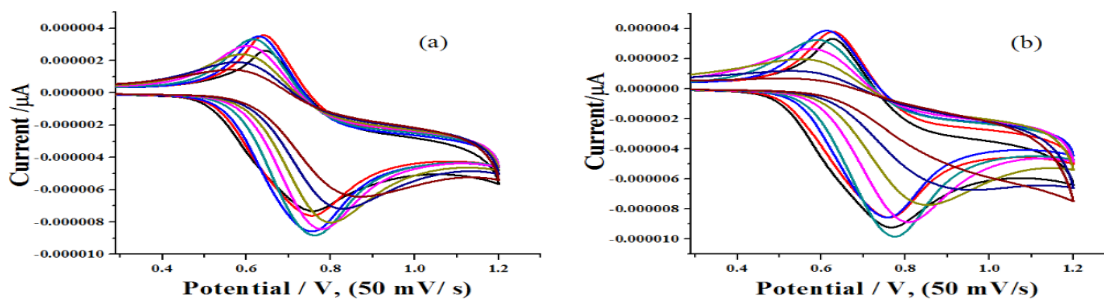


Fig. 10. CV titration study of R1 and Cd²⁺ ions [50 mV/s] under a) equimolar b) multimolar conditions

The changes noticed in the I_{pa} values (Table 2) for the addition of different metal ions with $10^{-3}M$ concentration (Fig. 11) and experiential magnified ΔE_p amount (111-138 mV) discloses the different binding ability of metal cation and also the effect of electrostatic repulsion operated between the oxidized ferrocene moiety and

bonded metal cations²⁷. Accessing the differences (ΔI_{pa} %) between the I_{pa} values noticed for the Fe^{II}/Fe^{III} oxidation wave of receptor solution and different metal ions added receptor solutions, uncover the coordination order of R1 as Hg²⁺ (81) > Pb²⁺ (17) > Ni²⁺ (15.7) > Mn²⁺ (12.8) > Cd²⁺ (4.2) > Cu²⁺ (3.7).

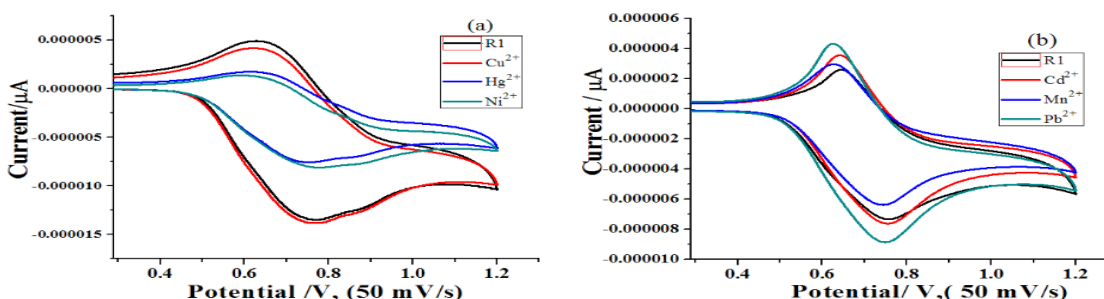


Fig. 11. Cyclic voltammograms recorded for various metal ions with R1 [50 mV/s] in a) acetonitrile b) ethanol

Table 2: Electrochemical data for equimolar titration (R1, $10^{-3} M/M^{2+}$, $10^{-3} M$) (Scan Rate 50 mV/ sec)

Addition	E_{pa} (V)	E_{pc} (V)	ΔE_p (V)	$E_{1/2}$ (V)	$I_{pa} \times 10^{-5}$ (μA)	$I_{pc} \times 10^{-6}$ (μA)
Solvent - Acetonitrile						
Receptor	0.766	0.63	0.136	0.698	-1.352	4.959
Hg ²⁺	0.754	0.622	0.132	0.688	-7.458	1.752
Cu ²⁺	0.766	0.628	0.138	0.697	-1.386	4.112
Ni ²⁺	0.762	0.619	0.142	0.691	-1.139	3.217
Solvent - Ethanol						
Receptor	0.756	0.644	0.111	0.7	-7.303	2.627
Cd ²⁺	0.754	0.64	0.113	0.697	-7.624	3.591
Mn ²⁺	0.745	0.624	0.121	0.685	-6.361	2.985
Pb ²⁺	0.748	0.624	0.124	0.686	-8.869	4.353

For multimolar concentration, witnessed (Table 3) binding power based on declining in ΔI_{pa} (%) of oxidation tendency of metal ion coupled with R1 is Cu²⁺ (86.07) > Hg²⁺ (85.6) > Ni²⁺ (85.47) > Cd²⁺ (15.4) > Mn²⁺ (81.96) > Pb²⁺ (83.15). Comparison of sensing priority of R1 towards several metal ions at homo and hetero molecular concentrations divulge R1 is effective towards Cu, Hg, and Ni ions at higher concentration of metal salts and at lower concentration adept lead for Hg, Pb and Ni ions (Figure 12).

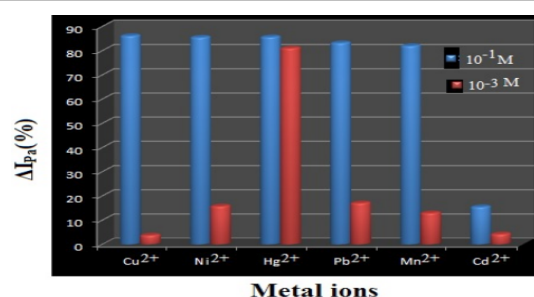


Fig. 12. Comparison of sensing ability of R1 and metal ion concentration

Table 3: Electrochemical data for multimolar titration (R1, 10^{-3} M/M $^{2+}$, 10^{-1} M) (Scan Rate-50 mV/ sec)

Addition	E_{pa} (V)	E_{pc} (V)	ΔE_p (V)	$E_{1/2}$ (V)	$I_{pa} \times 10^{-6}$ (μA)	$I_{pc} \times 10^{-6}$ (μA)
Solvent - Acetonitrile						
Receptor	0.766	0.63	0.136	0.698	-1.352	4.959
Hg $^{2+}$	0.791	0.638	0.152	0.714	-9.39	3.592
Cu $^{2+}$	0.801	0.642	0.159	0.722	-9.709	2.47
Ni $^{2+}$	0.774	0.651	0.123	0.712	-9.31	2.231
Solvent - Ethanol						
Receptor	0.756	0.644	0.111	0.7	-7.303	2.627
Cd $^{2+}$	0.764	0.628	0.136	0.696	-8.63	3.869
Mn $^{2+}$	0.793	0.603	0.19	0.698	-1.317	6.233
Pb $^{2+}$	0.781	0.607	0.173	0.694	-1.23	4.393

Like R1, R2 also display same trend (Table 4) in the values of ΔE_p , I_{pa} and I_{pc} upon scanning with different scan rate.

Homo molar (10^{-3} , R2/ 10^{-3} , M $^{2+}$) and hetero molar (10^{-3} , R2/ 10^{-1} , M $^{2+}$) titration studies (Fig.13) exemplify similar sensing behavior to metal ions. Calculated ΔI_{pa} (%) values depict, fastening trend for R2 under same molar condition as Pb $^{2+}$ (81.3)>Cu $^{2+}$ (76.8)> Mn $^{2+}$ (73.35)>Ni $^{2+}$ (23.6)> Cd $^{2+}$ (22.12)>Hg $^{2+}$ (8.4) (Table 5) and for different molar it is Cd $^{2+}$ (82.1)>Mn $^{2+}$ (80.4)>Pb $^{2+}$ (79)>Cu $^{2+}$ (26.1)>Ni $^{2+}$ (22.3)>Hg $^{2+}$ (18.1) (Table 6). Above observation relate that R2 shows better recognition

to Pb, Cu and Mn ions at lower concentration. Higher quantity of Cd $^{2+}$ is requisite for finding (Figure 14).

Antimicrobial Studies

Disc diffusion method (Mueller Hinton Agar base) was adopted to discover antibacterial activity of R1 & R2 against *Streptococcus faecalis*, *Staphylococcus aureuse*, *Salmonella typhimurium* and *Escherichia coli* (Fig.15). Likewise, anti-fungal studies for fungi *Candida albicans* and *Aspergillus niger* was done using Sabouraud's Dextrose agar as base (Fig.16). Table 7 highlights the zone of inhibition in mm perceived for the synthesized compounds R1 & R2 in antimicrobial analysis.

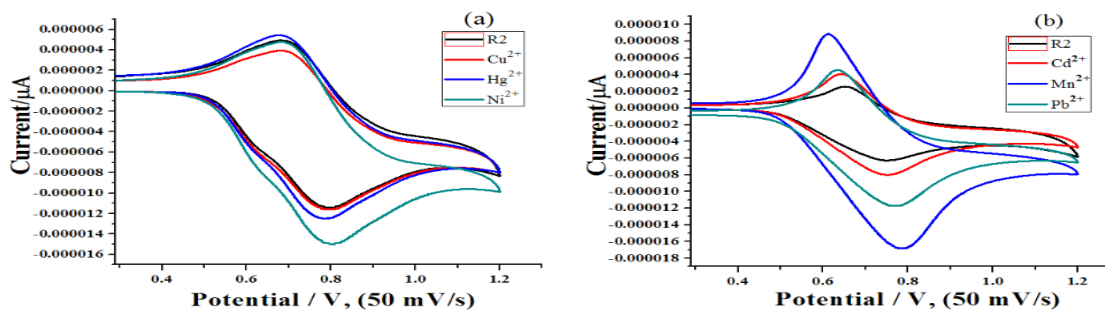


Fig. 13. Changes in CV of R2 upon addition of different metal ion [50 mV/s] a) acetonitrile b) ethanol

Table 4: Electrochemical parameters for R2

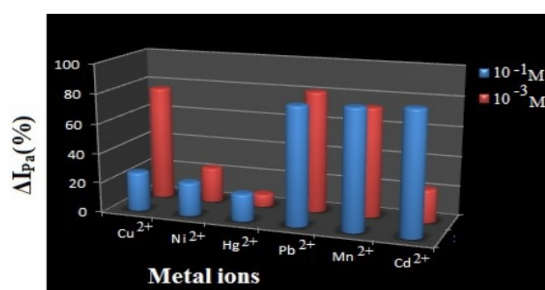
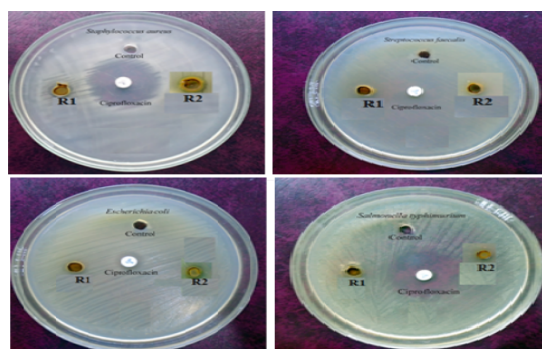
Scan Rate-mV/sec	E_{pa} (V)	E_{pc} (V)	ΔE_p (V)	$E_{1/2}$ (V)	$I_{pa} \times 10^{-5}$ (μA)	$I_{pc} \times 10^{-6}$ (μA)
Solvent - Acetonitrile						
20	0.787	0.683	0.103	0.735	-0.746	2.822
50	0.795	0.685	0.109	0.74	-1.137	4.846
100	0.797	0.683	0.113	0.74	-1.628	7.525
Solvent - Ethanol						
20	0.741	0.648	0.092	0.695	-0.397	0.681
50	0.75	0.651	0.099	0.7	-0.638	2.531
100	0.766	0.642	0.124	0.704	-1.037	5.328

Table 5: CV data for homo molar titration (R2, 10^{-3} M/M $^{2+}$, 10^{-3} M) (Scan Rate-50 mV/ sec)

Addition	E_{pa} (V)	E_{pc} (V)	ΔE_p (V)	$E_{1/2}$ (V)	$I_{pa} \times 10^{-5}$ (μA)	$I_{pc} \times 10^{-6}$ (μA)
Acetonitrile- solvent						
Receptor	0.799	0.685	0.113	0.742	-1.143	4.888
Hg $^{2+}$	0.785	0.675	0.109	0.73	-1.248	5.426
Cu $^{2+}$	0.799	0.685	0.113	0.742	-1.152	3.961
Ni $^{2+}$	0.803	0.681	0.121	0.742	-1.498	4.849
Ethanol – solvent						
Receptor	0.75	0.651	0.099	0.7	-6.277	2.593
Cd $^{2+}$	0.752	0.642	0.109	0.697	-8.057	4.05
Mn $^{2+}$	0.781	0.613	0.167	0.697	-1.672	8.89
Pb $^{2+}$	0.774	0.634	0.14	0.704	-1.172	4.565

Table 6: CV data for hetero molar titration (R2, 10^{-3} M/M $^{2+}$, 10^{-1} M) (Scan Rate-50 mV/sec)

Addition	E_{pa} (V)	E_{pc} (V)	ΔE_p (V)	$E_{1/2}$ (V)	$I_{pa} \times 10^{-5}$ (μA)	$I_{pc} \times 10^{-6}$ (μA)
Solvent -Acetonitrile						
Receptor	0.799	0.685	0.113	0.742	-1.143	4.888
Hg $^{2+}$	0.795	0.659	0.136	0.727	-1.397	5.451
Cu $^{2+}$	0.797	0.661	0.136	0.729	-1.548	5.785
Ni $^{2+}$	0.777	0.659	0.117	0.718	-1.473	5.653
Solvent -Ethanol						
Receptor	0.75	0.651	0.099	0.7	-6.277	2.593
Cd $^{2+}$	0.777	0.6221	0.154	0.699	-1.117	5.803
Mn $^{2+}$	0.756	0.624	0.132	0.69	-1.226	5.649
Pb $^{2+}$	0.768	0.619	0.148	0.694	-1.306	7.112

**Fig. 14. Comparison of binding ability of R2 and metal ion concentration****Fig. 16. Zone of inhibition for a) *Candida albicans* b) *Aspergillus niger*****Fig. 15. Zone of inhibition for a) *Streptococcus faecalis*, b) *Staphylococcus aureus*, c) *Salmonella typhimurium* and d) *Escherichia coli***

Defense mechanism rendered by R1 and R2 to prevent the growth of fungus *Aspergillus niger* is nearly 150 to 160% higher than that of the value witnessed for the standard Ketoconazole, which is unusual. Fungus *Candida albicans* progress is also prevented up to 50% of the standard value. Above result discloses that the compound R1 can be examined for antifungal agents formulation as there are only minimum numbers of antifungal agents available in the market¹⁵. Retardant nature of R1 & R2 displayed for two *Gram-positive* and two *Gram-negative* bacteria are on par with standard Ciprofloxacin.

Table7: In-vitro antimicrobial studies data

S.No	Microorganisms	Control	R1	R2	Ciprofloxacin/ Ketoconazole
zone of inhibition in mm for bacteria					
1	<i>Staphylococcus aureus</i>	-	10	8	25
2	<i>Streptococcus faecalis</i>	-	6	-	24
3	<i>Escherichia coli</i>	-	8	7	12
4	<i>Salmonella typhimurium</i>	-	8	6	27
zone of inhibition in mm for fungi					
1	<i>Candida albicans</i>	-	10	10	25
2	<i>Aspergillus niger</i>	-	12	13	8

Molecular docking studies

The purpose of molecular docking is to determine the mode of interaction of the complex protein-ligand. Docking results arrived are presented in the Table 8. For selected fungi and bacteria, ligand R1 binding 3D and 2D views (Fig. 17) and ligand R2 binding 3D and 2D views (Fig. 18) are presented. The binding scores for both the compounds fall between -3.61 to -7.45 Kcal mol⁻¹. Compound R1 exhibited better binding affinity with the protein 6KVQ (-6.52 Kcal

mol⁻¹) and R2 showed higher binding affinity with proteins 3K4Q and 7BU2 with -7.32 and -7.45 Kcal.mol⁻¹ respectively. Proteins 3K4Q & 6TZ6 are present in fungi, whereas protein 7BU2 is present in bacteria. Both the compounds R1 and R2 tested were involved in H-bond against active site residue 47 ILE, 50 PHE, 59 VAL, 60 ILE and 155 THR. Above results confirm that such type of ligand would represent a promising class for further development of a new class of antimicrobial agents which deserves further exploration.

Table 8: Results obtained from molecular docking studies

PDB	Free binding energy, kcal mol ⁻¹		R1		R2	
	R1	R2	Hydrogen bonds with receptor amino acids	Distance (Å)	Hydrogen bonds with receptor amino acids	Distance (Å)
1PTF	-3.61	-4.69	30-TYR	3.93	23-VAL	3.44
			50-PHE	3.69	24-GLN	3.95
			59-VAL	3.88	28-LYS	3.80
			60-ILE	3.98	47-ILE	3.66
			114-PHE	3.23		
3K4Q	-4.18	-7.32	45-LYS	3.04	27-GLN	3.91
			47-ILE	2.15	277-LYS	3.55
					278-LYS	3.37
4YXB	-5.21	-6.54	22-VAL	3.90	26-ALA	3.67
			155-THR	3.19	28-ILE	3.83
			157-GLU	3.56	29-PRO	3.78
			190-LEU	3.70	46-ILE	3.27
			225-LEU	3.30	51-ARG	3.23
6KVQ	-6.52	-5.26	153-LYS	2.27	188-ASN	3.32
			155-THR	3.05	189-VAL	3.50
			192-ASN	3.27		
			198-GLY	3.76		
6TZ6	-5.23	-6.3	103-ASP	2.95	50-PHE	3.84
			142-ARG	2.73	59-VAL	3.74
			142-ARG	2.79	60-ILE	3.65
7BU2	-5.48	-7.45	50-PHE	3.84	97-TYR	3.72
			59-VAL	3.74	42-HIS	3.64
			60-ILE	3.65	180-LEU	3.85
					240-ASN	3.31
					332-ARG	3.75

Exaggerated antifungal activities identified in *in-vitro* studies and high free binding energy values observed in molecular docking studies for fungus *Aspergillus niger*, provoke the rhythm of pharmaceutical research to be under taken.

ACKNOWLEDGEMENT

The authors acknowledge the support from

Dr. K. Pandian, Professor of Inorganic Chemistry & Controller of Examinations, University of Madras for the UV-Visible spectral studies free of cost. The research scholar D. Saranya wishes to record her thanks to the State Government of Tamil Nadu, India for the annual research assistant grant.

Conflicts of interest

“There are no conflicts to declare”.

REFERENCES

- Lu, Y.; Liang, X.; Niyungeko, C.; Zhou, J.; Xu, J.; Tian, G. *Talanta*, **2018**, *178*, 324–338. <http://dx.doi.org/10.1016/j.talanta.2017.08.033>.
- a) Bansod, B.; Kumar, T.; Thakur, R.; Rana, S.; Singh, I. *Biosensors & Bioelectronics*, **2017**, *94*, 443-455 <http://dx.doi.org/10.1016/j.bios.2017.03.031>. b) Wright, A. T.; Anslyn, E. V. *Chem. Soc. Rev.*, **2006**, *35*, 14–28. <http://dx.doi.org/10.1039/B505518K>. c) Lee, J. H.; Wang, Z.; Liu, J.; Lu, Y. *J. Am. Chem. Soc.*, **2008**, *130*, 14217–14226. <http://dx.doi.org/10.1021/ja803607z>.
- a) Xu, L.-W.; Wang, X.-T.; Zou, Y.-H.; Yu, X.-Y.; Xie, C.-Z.; Qiao, X.; Xu, J.-Y. *Appl Orgamet Chem.*, **2020**, *e5812*, 1-15. <https://doi.org/10.1002/aoc.5812>. b) Shaya, A.-R.; İpek O.; Doğan, E.; Mahmut, D. *Turkish Journal of Chemistry*, **2020**, *44*, 1254-1264. <https://doi.org/10.3906/kim-2004-68>.
- a) Andrea, B.; Vito, L. *Coordination Chemistry Revie.*, **2012**, *256*, 149–169 <http://dx.doi.org/10.1016/j.ccr.2011.05.015>. b) Smith, D. G.; Topolnicki, I. L.; Zwicker, V. E.; Jolliffe, K. A.; New, E. J. *Royal Society of Chemistry*, **2017**, *142*(19), 3544-3563. <http://dx.doi.org/10.1039/c7an01200d>.
- Lee, J. J.; Choi, Y. W.; You, G. R.; Lee, S. Y.; Kim, C. *Dalton Trans.*, **2015**, *44*, 13305-13314. <http://dx.doi.org/10.1039/c5dt00957j>.
- a) Mondal, A.; Roy Chowdhury, A.; Bhuyan, S.; Mukhopadhyay, S. K.; Banerjee, P. *Dalton Trans.*, **2019**, *c8dt05097j*, 1-12. <http://dx.doi.org/10.1039/c8dt05097j>. b) Qi, X.; Jun, E. J.; Xu, L.; Kim, S.-J.; Joong Hong, J. S.; Yoon, Y. J.; Yoon, J. *J. Org. Chem.*, **2006**, *71*, 2881-2884. <http://dx.doi.org/10.1021/jo052542a>.
- a) Ahmad Wani, M.; Thakur, N.; Pandey, M. D.; Pandey, R. *New Journal of Chemistry*, **2017**, *41*(18), 10000–10008. <http://dx.doi.org/10.1039/C7NJ02097J>. b) Gaetke, L.; Ching Kuang., *Toxicology*, **2003**, *189*, 147-163. [http://dx.doi.org/10.1016/S0300-483X\(03\)00159-8](http://dx.doi.org/10.1016/S0300-483X(03)00159-8).
- a) Vinita, B.; Valeria M, Nurchi.; Suban, K.; Sahoo., *Pharmaceuticals*, **2021**, *14*, 123(1-45). <https://doi.org/10.3390/ph14020123> b) Zapata, F.; Caballero, A.; Molina, P.; Tarraga, A. *Tarraga. Senso.*, **2010**, *10*, 11311-11321. <http://dx.doi.org/10.3390/s101211311>.
- Goswami, S.; Chakraborty, S.; Paul, S.; Halder, S.; Maity, A. C., *Tetrahedron Lett.*, **2013**, *54*, 5075–5077. <https://doi.org/10.1016/j.tetlet.2013.07.051>.
- Ellez-P; Navas-Acien, M.; Crainiceanu, A.; C, M.; Guallar, E., *Environ. Health Perspect.*, **2008**, *116*, 51–56. <https://doi.org/10.1289/ehp.10764>.
- Sunnapu, O.; Kotla, N. G.; Maddiboyina, B.; Singaravavel, S.; Sivaraman, G. *RSC Adv.*, **2016**, *6*, 656-660. <https://dx.doi.org/10.1039/c5ra20482h>.
- Aschner, M.; Guilarte, T. R.; Schneider, J. S.; Zheng, W. *Toxicology and Applied Pharmacology*, **2007**, *221*(2), 131–147. <https://doi.org/10.1016/j.taap.2007.03.001>.
- Ragavi, V.; Reshma, J.; Ananthi, M. *Organic & Medicinal Chem I J.*, **2018**, *5*(3), 1-6. <https://dx.doi.org/10.19080/OMCIJ.2018.05.555662>.
- Sinha, D.; Tiwari, A. K.; Singh, S.; Shukla, G.; Mishra, P.; Chandra, H.; Mishra, A. K. *Journal of Medicinal Chemistry*, **2008**, *43*, 160-165. <https://doi.org/10.1016/j.ejmech.2007.03.022>
- a) Buda De Cesare, G.; Cristy, S. A.; Garsin, D. A.; Lorenz, M. C. *mBio.*, **2020**, *11*(6), e02123-20. <https://dx.doi.org/10.1128/mbio.02123-20> b) Azevedo, M. M.; Teixeira-Santos, R.; Silva, A. P.; Cruz, L.; Ricardo, E.; Pina-Vaz, C.; Rodrigues, A. G. *Microbiology*, **2015**, *6*, 669(1-7). <https://dx.doi.org/10.3389/fmicb.2015.00669>.
- Mohamed, A. M.; Mohamed, E. K.; Koketsu, M. *American Journal of Chemistry*, **2012**, *2*(2), 38-51. <https://dx.doi.org/10.5923/j.chemistry.20120202.09>.

17. Bagamboula, C.F.; Uyttendaele, M.; Debevere, *J. Food Microbiology*, **2004**, *21*, 33-42. [https://dx.doi.org/10.1016/s0740-0020\(03\)00046-7](https://dx.doi.org/10.1016/s0740-0020(03)00046-7).
18. Morris, G.M.; Huey, R.; Lindstrom, W.; Sanner, M. F.; Belew, R. K.; Goodsell, D.S.; Olson, A.J. *J. of Computational Chem.*, **2009**, *30*, 2785-2791. <https://dx.doi.org/10.1002/jcc.21256>.
19. Constantinescu, C.; Matei, A.; Ion, V.; Mitu, B.; Ionita, I.; Dinescu, M.; Emandi, A. *Applied Surface Science.*, **2014**, *302*, 83–86. <http://dx.doi.org/10.1016/j.apsusc.2013.11.147>.
20. a) Gryaznova, T. P.; Katsyuba, S. A.; Milyukov, V. A.; Sinyashin, O. G. (2010). *J. of Organomet. Chem.*, **2010**, *695*, 2586–2595. <https://dx.doi.org/10.1016/j.jorganchem.2010.08.031> b) Sarhan, A. A. O.; Ibrahim, M. S.; Kamal, M. M.; Mitobe, K.; Izumi, T. *Monatshefte Für Chemie-Chemical Monthly.*, **2008**, *140*, 315–323 <https://dx.doi.org/10.1007/s00706-008-0025-2>.
21. Abi, M.; Subroto, C.; Suwarno. *Energies.*, **2018**, *11*, 364(1-12). <https://doi.org/10.3390/en11020364>.
22. Pandey, R.; Gupta, R. K.; Shahid, M.; Maiti, B.; Misra, A.; Pandey, D. S. *Inorg. Chem.*, **2012**, *51*, 298-311. <https://dx.doi.org/10.1021/ic201663m>.
23. Benramdane, R.; Benghanem, F.; Ourari, A.; Keraghel, S.; Bouet, G. *J. Coord. Chem.*, **2015**, *68*, 560-572. <https://dx.doi.org/10.1080/00958972.2014.994514>.
24. Kamatchi, P.; Selvaraj S.; Kandaswamy, M. *Polyhedron.*, **2005**, *24*, 900-908. <https://dx.doi:10.1016/j.poly.2005.02.012>.
25. Li, M.; Wang, R.; *Earth Environ. Sci.*, **2017**, *61*, 012043(1-5). <https://dx.doi.org/10.1088/1755-1315/61/1/012043>.
26. Alfonso, M.; Tárraga, A.; Molina, P. *Dalton Trans.*, **2010**, *39*, 8637–8645. <https://dx.doi.org/10.1039/c0dt00450b>
27. Kamal, A., Kumar, S.; Kumar, V.; Mahajan, R. K. *Sensors and Actuators B: Chemical.*, **2015**, *22*, 370–378. <https://dx.doi.org/10.1016/j.snb.2015.06.147>.